PRINT ISSN 1119-8362
Electronic ISSN 2659-1499

Full-text Available Online at
https://www.ajol.info/index.php/jasem
https://www.bioline.org.br/ja

J. Appl. Sci. Environ. Manage.
Vol. 30 (10B Supplementary) 4094-4102 Oct. 2026

Spatiotemporal Flood Dynamics and Hazard Mapping in the River Manafwa Catchment, Eastern Uganda (2004–2024)

[1]TURYAHABWE, R; [1]*WAMONO, E; [2]ANDAMA, E; [3]KIZZA-NKAMBWE, S

[1]Department of Geography, Faculty of Science and Education, Busitema University, P.O. Box 236, Tororo, Uganda;
[2]Department of Biology, Faculty of Science and Education, Busitema University, P.O. Box 236, Tororo, Uganda;
[3]Department of Engineering and Environment, Faculty of Engineering, Design and Technology, Uganda Christian University, P.O. Box 4, Mukono, Uganda.

**Corresponding Author Email: wamonoe3@gmail.com*
**ORCID: https://orcid.org/0000-0002-5411-8376*
**Tel: +256 778 249 625*

Co-authors Emails: tremmy082@gmail.com ; andamaedward@gmail.com ; kizzasa@gmail.com

ABSTRACT: Flooding is a recurrent hazard in eastern Uganda, yet long-term evidence on its spatial and temporal patterns in the River Manafwa catchment is limited. This study assessed flood dynamics from 2004 to 2024 and mapped flood hazard using satellite imagery, elevation, rainfall, land-cover, soil and historical flood information. Floodwater delineation combined optical water indices and Sentinel-1 backscatter; Mann–Kendall tests, Sen's slope, spatial autocorrelation statistics and an Analytical Hierarchy Process-based overlay were applied. Reported annual flood extent increased significantly (τ=0.67, $p<0.001$), with Sen's slope of 13.8 km² year^{-1}; flood frequency increased by 0.29 events year^{-1}. Flood occurrence was spatially clustered (Moran's I=0.487, $p<0.001$), particularly in middle and lower catchment river corridors and floodplains. High and very high hazard classes comprised 47.4% of the mapped assessment area, and the reported receiver-operating-characteristic area under the curve was 0.88. These findings suggest increasing flood pressure and identify priority areas for land-use planning, catchment protection, early-warning systems and preparedness.

DOI : https://dx.doi.org/10.4314/jasem.v30i10.68

License: CC-BY-4.0

Open Access Policy: All articles published by **JASEM** are open-access and free for anyone to download, copy, redistribute, repost, translate and read.

Copyright Policy: © 2026. Authors retain the copyright and grant **JASEM** the right of first publication. Any part of the article may be reused without permission, provided that the original article is cited.

Cite this Article as: TURYAHABWE, R; WAMONO, E; ANDAMA, E; KIZZA-NKAMBWE, S (2026). Spatiotemporal Flood Dynamics and Hazard Mapping in the River Manafwa Catchment, Eastern Uganda (2004–2024). *J. Appl. Sci. Environ. Manage*. 30 (10B Supplementary) 4094-4102

Dates: Received: 16 August 2026; Revised: 18 October 2026; Accepted: 22 October 2026; Published: 31 October 2026

Keywords: Flood frequency; Flood hazard; Geospatial analysis; Remote sensing; Spatio-temporal dynamics.

Floods are among the most frequent and destructive natural hazards globally, accounting for approximately 44% of disaster events and affecting more than 1.6 billion people between 2000 and 2019 (UNDRR, 2022). Their increasing frequency and intensity are associated with climate variability, land-use change, rapid urbanization and environmental degradation, with major consequences for life, infrastructure, agricultural productivity and ecosystem services (IPCC, 2021; WMO, 2021). Remote sensing and Geographic Information Systems (GIS) increasingly support flood-risk management by mapping flood extent, recurrence and hazard-prone areas (Tellman *et al.*, 2021). In Africa, flood impacts are amplified by deforestation, population growth, poor land use and limited hydrological monitoring (Douglas *et al.*, 2008; Adelekan, 2016; Winsemius *et al.*, 2016); more than 38 million people in Sub-Saharan Africa were affected between 2000 and 2022 (EM-DAT, 2023). East African highlands are increasingly exposed to flash floods because intense rainfall, steep slopes and catchment degradation generate rapid runoff (Ngecu and Mathu, 1999; Nicholson, 2017; Mahmoud and Gan, 2018). Uganda

**Corresponding Author Email: wamonoe3@gmail.com*
**ORCID: https://orcid.org/0000-0002-5411-8376*
**Tel: +256 778 249 625*

is particularly susceptible in its eastern highlands and downstream plains (NEMA, 2019, 2021). River Manafwa originates on Mount Elgon and traverses Bududa, Manafwa, Mbale and Butaleja districts before joining River Mpologoma. Floods reported in 2007, 2010, 2013, 2019 and 2022 caused deaths, displacement, crop loss and damage to roads, bridges and settlements (MWE, 2020; ReliefWeb, 2020; Office of the Prime Minister, 2022). Deforestation, cultivation on steep slopes, wetland encroachment and settlement expansion further alter catchment hydrology (Mugagga *et al.*, 2012), while experimental evidence from Uganda's highlands demonstrates substantial differences in soil loss among cropping systems and slope positions (Nabalegwa *et al.*, 2016).

Previous work in the Mount Elgon region has emphasized landslides, watershed degradation, water quality and community vulnerability (Mugagga *et al.*, 2012; Turyahabwe *et al.*, 2022). Studies in the neighbouring mountainous Sironko catchment also demonstrate relationships between land use, discharge, physicochemical water quality, habitat condition and fish communities (Turyahabwe *et al.*, 2020, 2022). Recent River Manafwa studies further show that agricultural, livestock-grazing, urban and riverbank-commercial stressors alter physicochemical water quality, heavy-metal concentrations and macroinvertebrate biological integrity (Wamono *et al.*, 2026a, 2026b). However, these ecological assessments did not quantify long-term flood frequency, extent and spatial hazard. This knowledge deficit sustains reactive management and constrains land-use planning, disaster preparedness and climate adaptation. Therefore, this study assessed flood dynamics and mapped hazard zones in the River Manafwa catchment by: (i) examining spatio-temporal flooding between 2004 and 2024; (ii) determining changes in flood frequency and extent; and (iii) identifying flood hazard zones using GIS and remote sensing. It hypothesized increasing flood occurrence, frequency and extent, with greater hazard in the downstream than upstream catchment.

MATERIALS AND METHODS

Study Area: The River Manafwa catchment lies on the western slopes of Mount Elgon in Eastern Uganda (approximately 0°45′–1°10′ N and 34°15′–34°40′ E), uses a mapped assessment area of approximately 1,755 km² in the submitted analysis (Table 3); the original watershed polygon was not available for independent verification and drains through Bududa, Manafwa, Mbale and Butaleja districts into River Mpologoma. Elevation declines from over 4,000 m above sea level on Mount Elgon to below 1,050 m in the Butaleja floodplains. Annual rainfall is approximately 1,200–2,500 mm in a bimodal regime, with March–May and September–November peaks. Steep upper slopes, intensive agriculture, deforestation, wetland encroachment and expanding settlements enhance runoff and flood susceptibility.

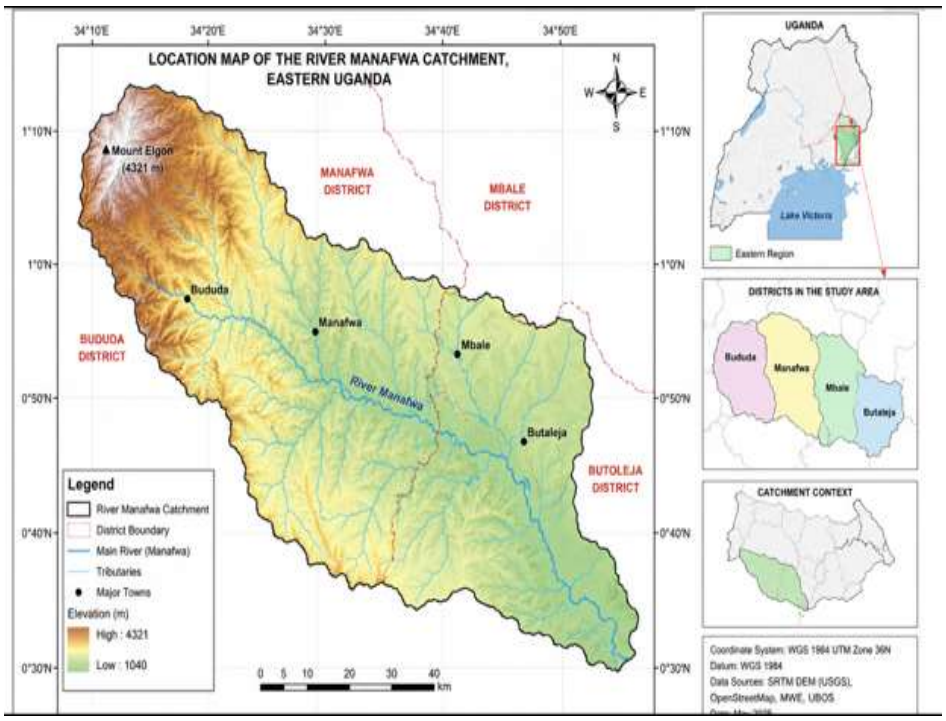


Fig. 1: Location of the River Manafwa catchment and its administrative setting.

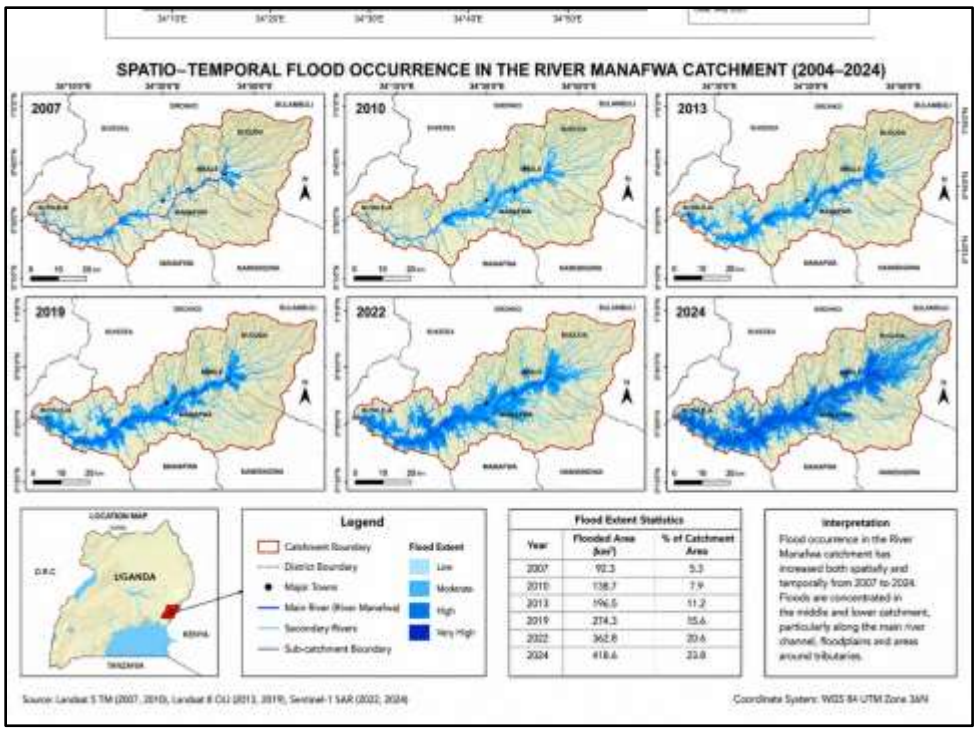


Fig. 2: Mapped flood occurrence in selected event years (2007, 2010, 2013, 2019, 2022 and 2024).

Data acquisition, preparation and flood delineation: Landsat 5 TM, Landsat 7 ETM+, Landsat 8 OLI, Sentinel-1 SAR and Sentinel-2 MSI scenes for representative flood years were obtained from USGS Earth Explorer and Copernicus. Peak-rainy-season and reported-event scenes were atmospherically, radiometrically and geometrically corrected, mosaicked, projected to WGS 1984 UTM Zone 36N and clipped to the catchment. Sentinel-1 processing included thermal-noise removal, radiometric calibration, speckle filtering and terrain correction. SRTM elevation, CHIRPS rainfall, FAO soil, classified land cover, OPM/NEMA disaster records, WorldPop population grids and GPS observations provided terrain, climatic, exposure and validation inputs (Table 1). Optical-image floodwater was extracted using the Normalized Difference Water Index (Eq. 1), where positive values denote water-covered surfaces.

$$NDWI = \frac{Green - NIR}{Green + NIR} \quad (1)$$

Sentinel-1 water was delineated by low-backscatter thresholding, enabling cloud-independent mapping. Annual binary flood rasters (F_i=1 flooded; 0 otherwise) were overlaid to compute flood frequency using Eq. 2 and classes of low (1–5), moderate (6–10), high (11–15) and very high (>15) occurrence.

$$Ff = \Sigma F_i \quad (2)$$

Flood areas were calculated in km², and the percentage change between successive periods was calculated using Eq. 3.

$$\%\Delta A = \left[\frac{A^2 - A^1}{A^1}\right] \times 100 \quad (3)$$

Temporal, spatial and hazard analyses: Mann–Kendall tests and Sen's slope quantified monotonic trends in annual flood extent and frequency; simple linear regression assessed change through time using R^2, F and p statistics. Global Moran's I tested spatial autocorrelation, while Getis–Ord Gi* identified 90%, 95% and 99% recurrent-flood hotspots. Analyses used ArcGIS Pro 3.2 and R 4.4.0 at α=0.05. Seven flood-conditioning factors—elevation, slope, drainage density, river distance, land use/land cover, rainfall and soil—were standardized to five susceptibility classes. Elevation and slope came from 30-m SRTM; drainage density was calculated using Eq. 4; river distance used Euclidean buffers; CHIRPS rainfall was interpolated by inverse-distance weighting; land cover used supervised Landsat classification; and soils were reclassified by infiltration capacity.

$$Dd = \frac{\Sigma L}{A} \quad (4)$$

Analytical Hierarchy Process pairwise comparison assigned weights (Table 1), with consistency accepted when the consistency ratio in Eq. 5 was below 0.10.

$$CR = \frac{CI}{RI} \quad (5)$$

The flood-hazard index was calculated using Eq. 6 and classified by Jenks natural breaks into very low, low, moderate, high and very high hazard.

$$FHI = \Sigma W_i X_i \quad (6)$$

Historical records, GPS points and field observations validated the model using a receiver-operating-characteristic curve and area under the curve (AUC), interpreted as poor (<0.70), good (0.70–<0.80), very good (0.80–<0.90) and excellent (≥0.90).

Table 1: Data inputs, applications and Analytical Hierarchy Process weights used in flood assessment.

Dataset/factor	Source/resolution	Application	AHP weight (%)
Landsat 5/7/8	USGS; 30 m	Historical flood and land-cover mapping	—
Sentinel-1 SAR	Copernicus; 10 m	Cloud-period flood extraction	—
Sentinel-2 MSI	Copernicus; 10 m	Recent flood validation	—
Slope	Derived from SRTM DEM; 30 m	Terrain-gradient influence on runoff	10
SRTM DEM/elevation	USGS; 30 m	Elevation, slope, flow and drainage	15
CHIRPS rainfall	Climate Hazards Center; 0.05°	Rainfall variability and intensity	25
River distance	Derived from river network	Proximity-related susceptibility	20
Drainage density	Derived from DEM	Runoff concentration	15
Land use/land cover	Landsat classification; 30 m	Surface cover influence	10
Soil type	FAO soil data; 1 km	Infiltration capacity	5
Historical flood records	OPM/NEMA and district reports	Occurrence and model validation	—
Population	WorldPop; 100 m	Exposure assessment	—
Field/GPS observations	Survey points	Ground-truth validation	—

RESULTS AND DISCUSSION

Spatiotemporal flood dynamics, frequency and extent: Fig. 2 shows recurrent but heterogeneous flooding during all selected years. In 2007, inundation was largely localized along the main River Manafwa channel and immediate floodplains; it expanded through tributaries and adjacent plains by 2013 and became widespread in 2019, 2022 and 2024. The middle and lower catchment especially Manafwa, Mbale and Butaleja consistently experienced the broadest inundation, whereas the steep Bududa uplands experienced localized flash flooding. Flood concentration along channels, confluences, wetlands and low-lying floodplains demonstrates the control of topography and drainage, while increasing coverage suggests contributions from rainfall variability, vegetation loss, cultivation, wetland encroachment and reduced infiltration. Across 21 observations, annual flood extent averaged 197.5 km² (SD=112.4; CV=56.9%), ranging from 55.6 to 418.6 km². Positive skewness (0.84) indicates fewer but influential large floods, whereas kurtosis of −0.61 reflects a flatter distribution containing moderate and extreme years. Extent rose from 55.6 km² (3.2% of the catchment) in 2004 to 418.6 km² (23.9%) in 2024, with the largest mapped increases after 2018 (Table 2). The Mann–Kendall trend was significant (τ=0.67, Z=3.84, p<0.001), and Sen's slope indicated an annual increase of 13.8 km². Linear regression (y=13.8x+46.2; R^2=0.74; F=54.6; p<0.001; SE=2.1 km² year^{-1}) corroborated progressive expansion. The inference that catchment degradation contributes to hydrological deterioration is consistent with evidence of cropping-system-related soil loss (Nabalegwa *et al.*, 2016), land-use and river-condition relationships in the Sironko catchment (Turyahabwe *et al.*, 2020, 2022), and locally observed declines in water quality and biological integrity under disturbed River Manafwa land uses (Wamono *et al.*, 2026a, 2026b). These ecological and erosion responses support the degradation pathway but do not independently establish flood causation. Annual flood frequency averaged 6.8 events (SD=3.4; CV=50.0%), ranged from 2 to 15 and increased significantly (τ=0.63, Z=3.57, p<0.001) by 0.29 events year^{-1}. Flood occurrence (τ=0.58, p=0.0013), magnitude (τ=0.61, p<0.001) and spatial expansion (τ=0.64, p<0.001) also increased. These trends show that flooding has become both more recurrent and spatially extensive, consistent with climate- and land-use-related increases reported elsewhere in East Africa (Mugagga *et al.*, 2012; Mahmoud and Gan, 2018).

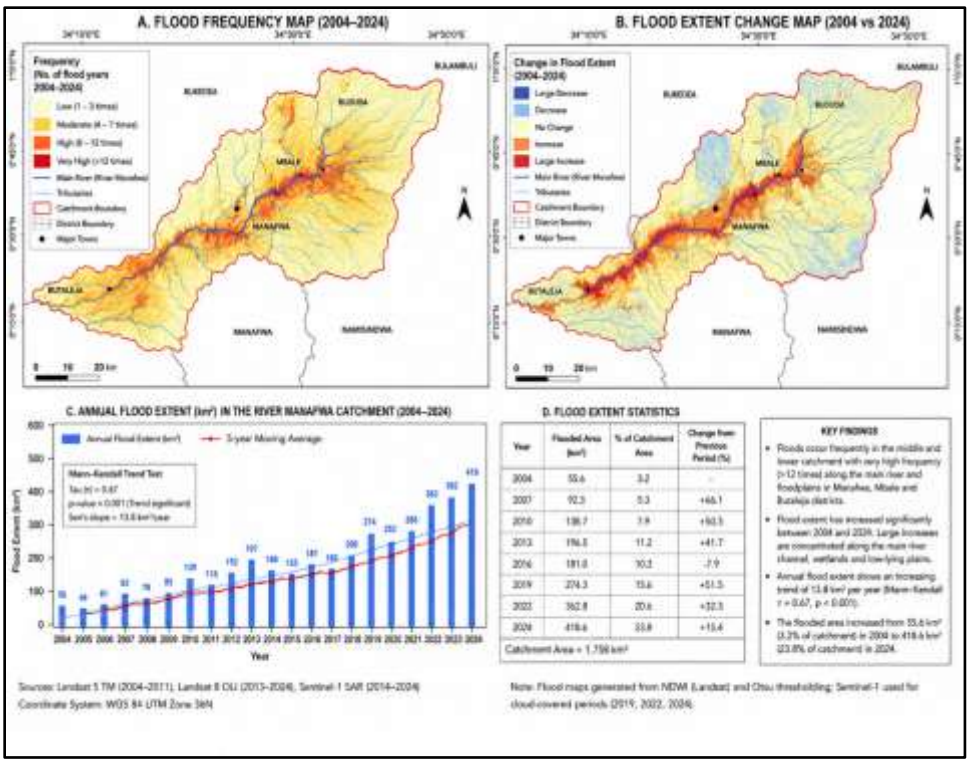


Fig. 3: Flood frequency, flood-extent change and temporal trend in the River Manafwa catchment.

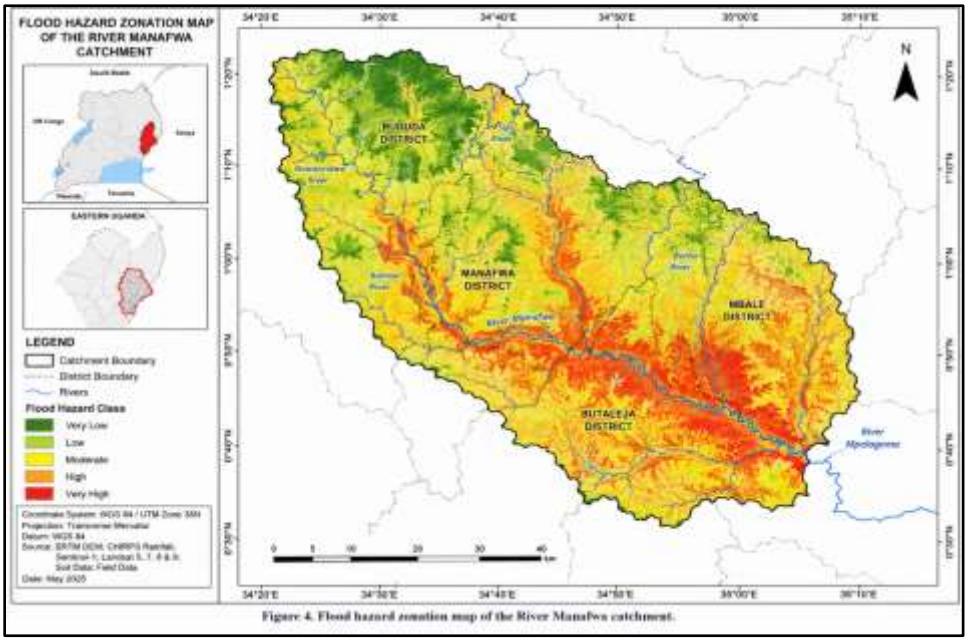


Fig. 4: Flood-hazard zonation in the River Manafwa catchment.

Spatial clustering and flood hotspots: Moran's I were 0.487 compared with an expected value of −0.031 (variance=0.007; Z=5.84; p<0.001), confirming significant spatial clustering rather than random distribution. Getis–Ord Gi* identified 18 hotspots at 90%, 13 at 95% and 9 at 99% confidence. The strongest clusters occurred along the middle and lower River Manafwa, Butaleja floodplains, tributary confluences and wetland systems (Fig. 3). Their low elevation, high drainage density, proximity to channels and capacity to receive accumulated runoff from Mount Elgon explain chronic exposure, paralleling clustered flood patterns in other tropical basins (Khosravi *et al.*, 2018; Khosravi *et al.*, 2018).

Table 2: Consolidated descriptive, trend, regression, hotspot and period flood statistics, 2004–2024.

Analysis/variable	n or period	Estimate/result	Z/F	p-value	Interpretation
Flood extent: descriptive	21	Mean 197.5; SD 112.4; min–max 55.6–418.6 km²; CV 56.9%; skew 0.84; kurtosis −0.61	—	—	High interannual variability
Flood frequency: descriptive	21	Mean 6.8; SD 3.4; min–max 2–15; CV 50.0%; skew 0.71; kurtosis −0.48	—	—	High temporal variability
Flood occurrence trend	2004–2024	τ=0.58; slope 0.11 events yr⁻¹	3.21	0.0013	Increasing
Flood extent trend	2004–2024	τ=0.67; slope 13.8 km² yr⁻¹	3.84	<0.001	Increasing
Flood magnitude trend	2004–2024	τ=0.61; slope 7.2 km² yr⁻¹	3.52	<0.001	Increasing
Spatial expansion trend	2004–2024	τ=0.64; slope 12.5 km² yr⁻¹	3.67	<0.001	Increasing
Flood frequency trend	2004–2024	τ=0.63; slope 0.29 events yr⁻¹	3.57	<0.001	Increasing
Linear regression	21	y=13.8x+46.2; R²=0.74; adjusted R²=0.72; SE=2.1	F=54.6	<0.001	Strong positive trend
Moran's I	—	Observed 0.487; expected −0.031; variance 0.007	5.84	<0.001	Significant clustering
Getis–Ord Gi* hotspots	—	90%: 18; 95%: 13; 99%: 9	—	<0.10/<0.05/<0.01	Moderate/significant/highly significant
Flooded area	2004	55.6 km²; 3.2%	—	—	Baseline
Flooded area	2007	92.3 km²; 5.3%; +66.1%	—	—	Expansion
Flooded area	2010	138.7 km²; 7.9%; +50.3%	—	—	Expansion
Flooded area	2013	196.5 km²; 11.2%; +41.7%	—	—	Expansion
Flooded area	2019	274.3 km²; 15.6%; +39.6%	—	—	Expansion
Flooded area	2022	346.8 km²; 19.7%; +26.4%	—	—	Expansion
Flooded area	2024	418.6 km²; 23.9%; +20.7%	—	—	Expansion

Flood hazard distribution, exposure, depth and velocity: The hazard model classified 17.0% (298.6 km²) as very high, 30.4% (533.8 km²) as high, 34.0% (596.5 km²) as moderate, 15.1% (264.7 km²) as low and 3.5% (61.4 km²) as very low (Table 3). Thus, high and very high classes together covered 47.4% of the catchment. The highest hazard followed River Manafwa, major tributaries, wetlands and confluences in Butaleja and parts of Manafwa and Mbale, whereas elevated Bududa terrain was mostly low or very low. Rainfall (25%) and river proximity (20%) were the dominant model factors, followed by elevation and drainage density (15% each), land cover (10%), slope (10%) and soil (5%). An estimated 186,450 people occupied very high hazard zones and 271,920 occupied high hazard zones; with 286,310 in moderate zones, these patterns expose settlements and intensive floodplain agriculture to repeated loss.

Flood depths above 3 m occurred along the main channel, confluences and downstream plains. Velocities above 2.0 m s⁻¹ occurred along the channel and narrow valleys, while slower laterally spreading water characterized wetlands and floodplains (Figs. 5 and 6). High depth increases inundation damage, whereas high velocity enhances erosion and structural failure; both should inform infrastructure siting and evacuation planning. Validation aligned historical and observed flood locations with predicted high and very high zones. The ROC AUC of 0.88 indicates very good predictive performance, supporting the integrated GIS/remote-sensing framework for hazard screening, early warning and catchment planning. Nevertheless, the model represents relative hazard from the selected datasets and weights; hydrodynamic simulation, future climate scenarios and socio-economic vulnerability would further refine risk estimates.

Study limitations: The original submitted manuscript gives an approximate catchment area of 1,200 km², whereas the hazard-class table reports a mapped assessment area of 1,754.9 km². The mapped flood percentages predominantly use the latter denominator; the source boundary polygon was unavailable for independent measurement. The hazard-class area rows sum to 1,755.0 km², a 0.1 km² difference from the stated total, plausibly caused by tabular rounding. The 2024 reported flood extent of 418.6 km² corresponds to approximately 23.9% of 1,754.9 km²; the original manuscript stated 23.8%, which has been corrected in the text and Table 2.

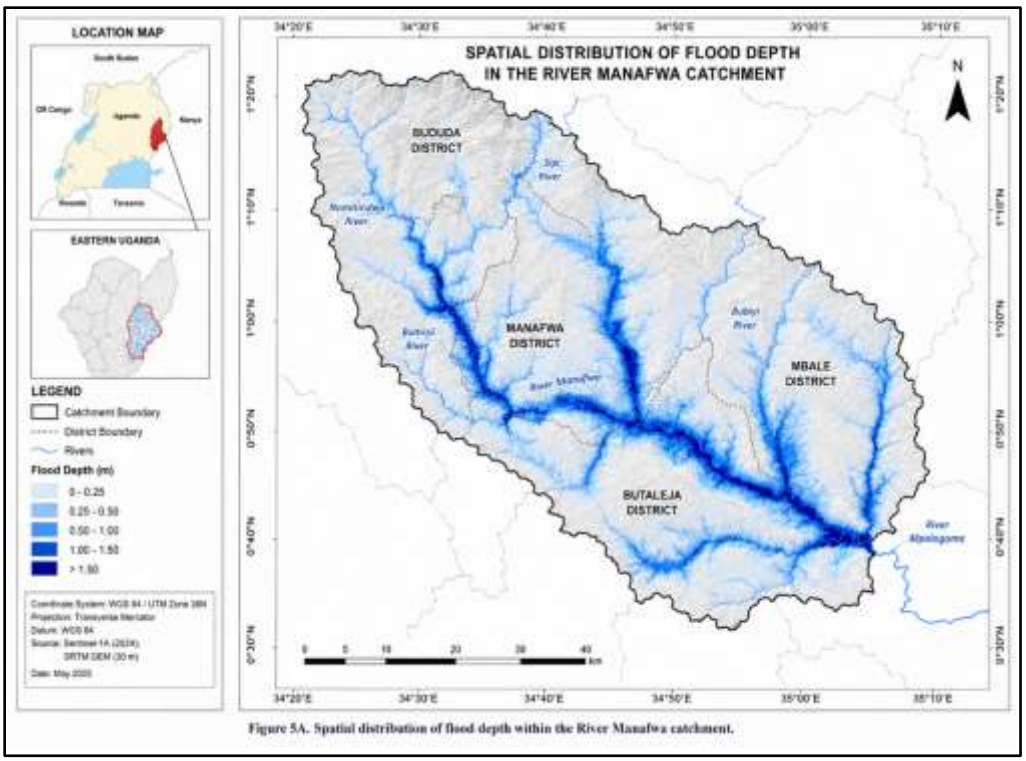


Fig. 5: Spatial distribution of mapped flood depth in the River Manafwa catchment.

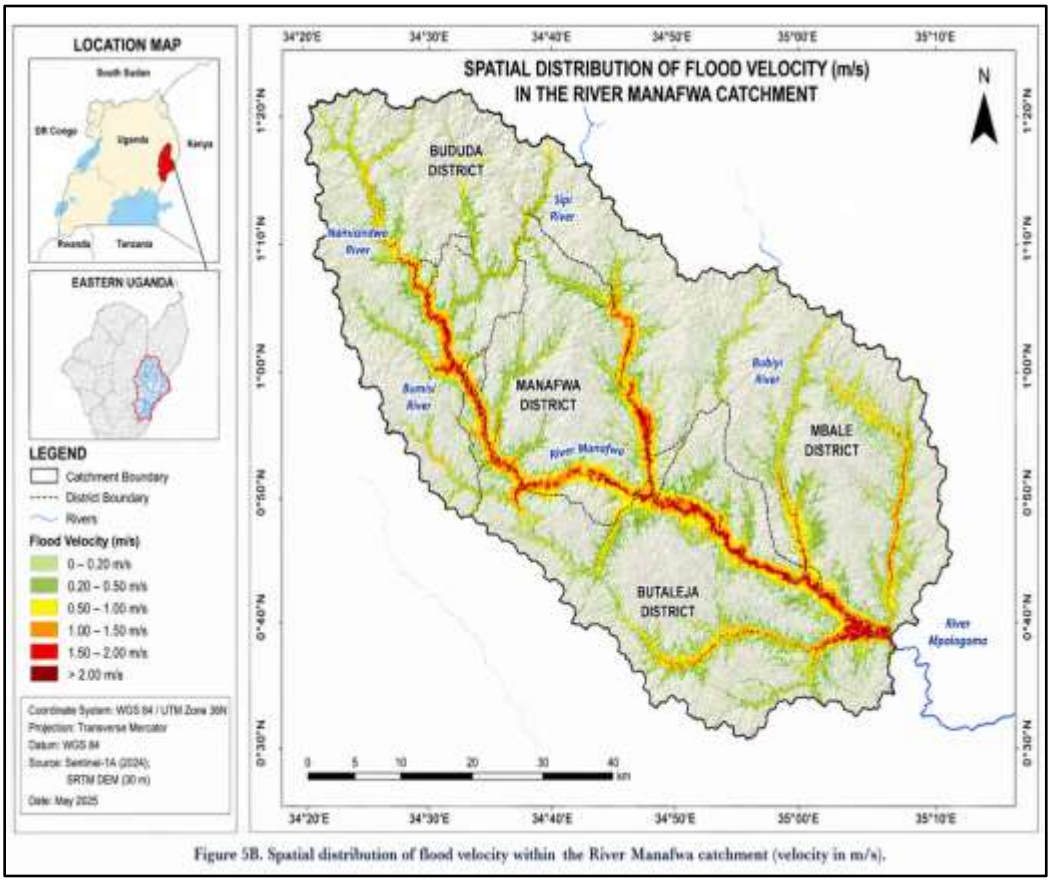


Fig. 6: Spatial distribution of mapped flood velocity in the River Manafwa catchment.

Table 3: Flood-hazard area, population exposure and model-performance summary.

Hazard class/metric	Area (km²)	Catchment (%)	Population exposed	Interpretation
Very high	298.6	17.0	186,450	River channels, wetlands and downstream floodplains
High	533.8	30.4	271,920	Extensive flood-prone lowlands
Moderate	596.5	34.0	286,310	Transitional hazard areas
Low	264.7	15.1	146,870	Elevated or better-drained terrain
Very low	61.4	3.5	51,240	Least susceptible terrain
Total	1,754.9	100	942,790	Mapped assessment area
ROC AUC	—	—	—	0.88: very good predictive performance

Original event-level flood records, underlying rasters, depth and velocity modelling outputs, AHP pairwise matrix and receiver-operating-characteristic validation data were not supplied for independent reproduction. Consequently, these findings are presented as outputs of the original submitted analysis rather than independently verified results. The flood-hazard overlay indicates relative susceptibility and should not be equated with a fully calibrated hydrodynamic flood model.

Conclusion: This study characterized changes in flood occurrence and delineated zones of relative flood hazard in the River Manafwa catchment. The mapped patterns indicate a concentration of flood pressure along river corridors and downstream floodplains, highlighting priorities for risk-sensitive land-use planning, wetland and catchment restoration, early warning and disaster preparedness. The integration of multi-sensor observations, temporal trends and spatial hazard screening provides a framework for catchment-scale planning. Interpretation remains constrained by the available flood-event records, map classification and model-validation inputs. Subsequent research should independently validate the historical time series and catchment boundary, and combine hydrodynamic modelling, climate projections and vulnerability assessments to improve operational flood-risk estimates.

DECLARATIONS

Ethical Approval: This study did not involve human participants or animal experimentation and therefore did not require formal ethical approval. All procedures involving data handling and analysis were conducted responsibly and in accordance with standard academic and institutional guidelines.

Disclaimer on artificial intelligence usage: Author(s) hereby declare that no generative Artificial Intelligence (AI) technologies such as Large Language Models (ChatGPT, COPILOT, XLNet, Ernie 3.0 Titan etc) and text-to-image generators have been used during writing or editing of this manuscript.

Acknowledgement: The author gratefully acknowledges the Department of Geography, Busitema University, for providing an enabling environment for this study. Appreciation is also extended to the Ministry of Water and Environment, Uganda National Meteorological Authority, National Environment Management Authority, and the Office of the Prime Minister for providing valuable information. Special thanks are due to the United States Geological Survey, Copernicus Open Access Hub, and CHIRPS for availing the geospatial datasets used in this study.

Declaration of Conflict of Interest: The authors declare that no known conflict of interest or personal relationships have influenced the work reported in this paper.

Declaration of Data Availability: Source geospatial products and processed analytical datasets should be requested from the corresponding author.

REFERENCES

Adelekan, IO (2016). Flood risk management in the coastal city of Lagos, Nigeria. J. *Flood Risk Manage*. 9(3): 255–264. DOI: https://doi.org/10.1111/jfr3.12179

Douglas, I; Alam, K; Maghenda, M; McDonnell, Y; McLean, L; Campbell, J (2008). Unjust waters: Climate change, flooding and the urban poor in Africa. *Environ. Urban*. 20(1): 187–205. DOI: https://doi.org/10.1177/0956247808089156

EM-DAT (2023). The International Disaster Database. Centre for Research on the Epidemiology of Disasters, Université Catholique de Louvain. https://www.emdat.be

Hosmer, DW; Lemeshow, S (2000). Applied Logistic Regression. 2nd Ed. John Wiley & Sons. Intergovernmental Panel on Climate Change (IPCC) (2021). Climate Change 2021: *The Phy. Sci. Basis. Cambridge Univer. Press*. DOI: https://doi.org/10.1017/9781009157896

Khosravi, K; Pham, BT; Chapi, K; Shirzadi, A; Shahabi, H; Revhaug, I; Prakash, I; Bui, DT (2018). A comparative assessment of decision trees algorithms for flash flood susceptibility modeling at Haraz watershed, northern Iran. *Sci. Total Environ*. 627: 744–755. DOI: https://doi.org/10.1016/j.scitotenv.2018.01.266

Mahmoud, SH; Gan, TY (2018). Urbanization and climate-change implications in flood-risk management: Developing an efficient decision-support system for flood-susceptibility mapping. *Sci. Total Environ*. 636: 152–167. DOI: https://doi.org/10.1016/j.scitotenv.2018.04.282

Ministry of Water and Environment (MWE) (2020). Uganda Water and Environment Sector Performance Report 2020. Ministry of Water and Environment, Kampala.

Mugagga, F; Kakembo, V; Buyinza, M (2012). Land use changes on the slopes of Mount Elgon and the implications for the occurrence of landslides. *Catena* 90: 39–46. DOI: https://doi.org/10.1016/j.catena.2011.11.004

Nabalegwa, MW; Asaba, J; Turyahabwe, R (2016). Soil loss under different cropping systems in highlands of Uganda. *Univ. J. Agric. Res*. 4(6): 217–229. DOI: https://doi.org/10.13189/ujar.2016.040601

National Environment Management Authority (NEMA) (2019). State of the Environment Report for Uganda 2018. NEMA, Kampala.

National Environment Management Authority (NEMA) (2021). State of the Environment Report for Uganda 2020. NEMA, Kampala.

Ngecu, WM; Mathu, EM (1999). El Niño-triggered landslides and their socioeconomic impact on Kenya. *Environ. Geol*. 38(4): 277–284. DOI: https://doi.org/10.1007/s002540050426

Nicholson, SE (2017). Climate and climatic variability of rainfall over Eastern Africa. *Rev. Geophys*. 55(3): 590–635. DOI: https://doi.org/10.1002/2016RG000544

Office of the Prime Minister (2022). Annual Disaster Report 2022. Government of Uganda, Kampala.

ReliefWeb (2020). Uganda: Floods and Landslides Situation Report. https://reliefweb.int

Saaty, TL (1980). The Analytic Hierarchy Process. McGraw-Hill, New York.

Tellman, B; Sullivan, JA; Kuhn, C; Kettner, AJ; Doyle, CS; Brakenridge, GR; Erickson, TA; Slayback, DA (2021). Satellite imaging reveals increased proportion of population exposed to floods. *Nature* 596: 80–86. DOI: https://doi.org/10.1038/s41586-021-03695-w

Turyahabwe, R; Mulinya, C; Shivoga, WA (2020). Influence of land use/cover on water quality in the River Sironko catchment area, Eastern Uganda. IOSR J. Environ. Sci. Toxicol. *Food Technol*. 14(8): 26–36. DOI: https://doi.org/10.9790/2402-1408012636

Turyahabwe, R; Mulinya, C; Shivoga, WA (2022). Relationships between land use, habitat quality, physicochemical water quality and fish communities in the Sironko River Catchment, a mountainous tropical stream flowing into Lake Kyoga in Eastern Uganda. *Lakes Reserv. Res. Manage*. 27(2): e12406. DOI: https://doi.org/10.1111/lre.12406

United Nations Office for Disaster Risk Reduction (UNDRR) (2022). Global Assessment Report on Disaster Risk Reduction 2022. United Nations, Geneva.

Wamono, E; Turyahabwe, R; Ochieng, H; Andama, E (2026a). Influence of forestry, agricultural, livestock grazing, urban land-use and car-washing point stressors on physicochemical characteristics, heavy-metal levels and water-quality variables during wet and dry seasons in River Manafwa Catchment, Eastern Uganda. *J. Appl. Sci. Environ. Manage.* 30(6): 2057–2065. DOI: https://doi.org/10.4314/jasem.v30i6.38

Wamono, E; Turyahabwe, R; Ochieng, H; Andama, E (2026b). Macroinvertebrate assemblage responses and biological integrity across contrasting anthropogenic stressors in River Manafwa Catchment, Eastern Uganda. *J. Appl. Sci. Environ. Manage*. 30(7): 2299–2310. DOI: https://doi.org/10.4314/jasem.v30i7.26

Winsemius, HC; Aerts, JCJH; van Beek, LPH; Bierkens, MFP; Bouwman, A; Jongman, B; Kwadijk, JCJ; Ligtvoet, W; Lucas, PL; van Vuuren, DP; Ward, PJ (2016). Global drivers of future river-flood risk. *Nat. Clim. Change* 6(4): 381–385. DOI: https://doi.org/10.1038/nclimate2893

World Meteorological Organization (WMO) (2021). State of the Climate in Africa 2020. WMO, Geneva.